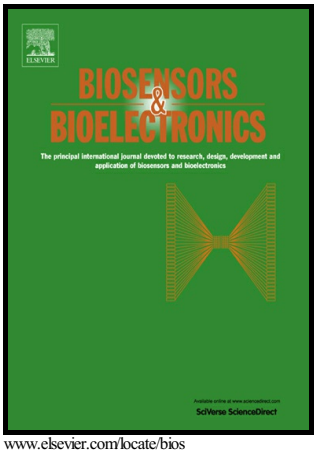

www.elsevier.com/locate/bios

Sensitive electrogenerated chemiluminescence biosensors for protein kinase activity analysis based on bimetallic catalysis signal amplification and recognition of Au and Pt loaded metal-organic frameworks nanocomposites

Zhiyong Yan, Feng Wang, Pingye Deng, Yu Wang, Kai Cai, Yanhui Chen, Zonghua Wang, Yang Liu

PII: S0956-5663(18)30168-4
DOI: https://doi.org/10.1016/j.bios.2018.03.004
Reference: BIOS10330

To appear in: *Biosensors and Bioelectronic*

Received date: 7 December 2017
Revised date: 22 February 2018
Accepted date: 1 March 2018

Cite this article as: Zhiyong Yan, Feng Wang, Pingye Deng, Yu Wang, Kai Cai, Yanhui Chen, Zonghua Wang and Yang Liu, Sensitive electrogenerated chemiluminescence biosensors for protein kinase activity analysis based on bimetallic catalysis signal amplification and recognition of Au and Pt loaded metal-organic frameworks nanocomposites, *Biosensors and Bioelectronic,* https://doi.org/10.1016/j.bios.2018.03.004

Sensitive electrogenerated chemiluminescence biosensors for protein kinase activity analysis based on bimetallic catalysis signal amplification and recognition of Au and Pt loaded metal-organic frameworks nanocomposites

Zhiyong Yan [a], *Feng Wang* [b], Pingye Deng [a]*, Yu Wang [a], Kai Cai [a], Yanhui Chen [a], *Zonghua Wang* [c], *Yang Liu* [b]*

[a] Beijing Center for Physical and Chemical Analysis, Beijing 100089, China.

[b] Department of Chemistry, Beijing Key Laboratory for Analytical Methods and Instrumentation, Key Lab of Bioorganic Phosphorus Chemistry and Chemical Biology of Ministry of Education, Tsinghua University, Beijing 100084, China.

[c] Shandong Sino-Japanese Center for Collaborative Research of Carbon Nanomaterials, College of Chemistry and Chemical Engineering, Qingdao Universiy, Qingdao, Shandong, 266071, China.

*Corresponding author.

Tel: 86-10-62798187; Fax: 86-10-62771149

E-mail addresses: liu-yang@mail.tsinghua.edu.cn, dengpy99@tsinghua.org.cn

Abstract

In this work, a novel and sensitive electrogenerated chemiluminescence (ECL) biosensor for protein kinase A (PKA) activity analysis and relevant inhibitor screening was proposed based on bimetallic catalysis signal amplification and recognition of Au and Pt nanoparticles loaded metal-organic frameworks (Au&Pt@UiO-66) nanocomposite. After being phosphorylated by PKA in the presence of ATP, Au&Pt@UiO-66 probes were specifically chelated to the modified electrode by forming Zr-O-P bonds between the surface defects of UiO-66 and the phosphorylated kemptide. Due to the high synergistic catalysis of Au&Pt@UiO-66 nanocomposites to the luminol-H_2O_2 reaction, the ECL signal of luminol was greatly enhanced. Moreover, UiO-66 afford numerous Zr defect sites for high efficient phosphate group recognition, and can also prevent the nanoparticles from aggregating during catalytic reactions. Thus, the excellent performance of the ECL biosensor with high sensitivity and superior stability was obtained. Under the optimized conditions, the detection limit for PKA activity was 0.009 UmL^{-1} (S/N=3). Meanwhile, the ECL biosensor was successfully applied in inhibitor screening and cell lysates PKA activity analysis, showing great promise in kinase related research.

Keywords: kinase activity, inhibitor screening, phosphoric group recognition, bimetallic catalysis, metal-organic frameworks

1. Introduction

Protein phosphorylation catalyzed by protein kinase and dephosphorylation catalyzed by phosphatase play important roles in intracellular signaling pathways (Hunter 2000). In principle, protein kinase can catalyze the phosphorylation of protein through transferring phosphate groups from nucleoside triphosphates (adenosine-5′-triphosphate, ATP) to the OH group of an amino acid side chain in peptides or protein substrate. As is well known, protein kinase is involved in a variety of cellular activities such as cell surface signal transduction (Nishizuka 1986), gene transcription (Whitmarsh 2007), metabolism (Whiteman et al. 2002), cellular proliferation (Zhang et al. 1990). Thus, the level of protein kinase activity can be considered as an indicator of many human diseases, such as diabetes (Evcimen and King 2007), Alzheimer's disease (Salminen et al. 2011), metabolic syndrome and heart disease (Hardie 2008). In addition, kinase inhibitors can regulate down the activity of protein kinase and have been widely investigated in medicinal research and clinical treatment (Hughes et al. 2006). Therefore, it is highly desirable to develop a sensing platform for the accurate protein kinase activity analysis and potential inhibitors screening.

Up to now, several methods have been developed to detect protein kinase activity such as isotope labeling technique (Hennrich et al. 2013), fluorescence (Colombo et al. 2017; Shen et al. 2015), colorimetry (Zhou et al. 2014) and electrochemical based analytical systems (Shen et al. 2016a), etc. (Liu et al. 2014). Among these methods, electrogenerated chemiluminescence (ECL) technique exhibits unique advantages (Ji et al. 2017; Zhu et al. 2017), such as low background, easy temporal and spatial controllability due to the intrinsic light-generation process of ECL on the electrode surface (Meng et al. 2016). For instance, an ECL biosensor for protein kinase A (PKA) activity detection was reported based on double-quenching of graphene quantum dots ECL by G-quadruplex-hemin DNAzyme and gold nanoparticles (AuNPs) (Liu et al. 2015a). AuNPs mediated dual-potential ECL ratiometric approach based on the simultaneous decrease of cathodic ECL from graphene quantum dots and

enhancement of anodic ECL from luminol was reported for protein kinase activity assay (Zhao et al. 2015). Ruthenium complex functionalized protein A and specific peptides were utilized as ECL probe and recognition substrates respectively in an ECL strategy for cyclic adenosine monophosphate-dependent protein kinase and casein kinase II detection (Liu et al. 2016). However, because of the limited phosphate group recognition sites, the metal ion chelation and antibody recognition can suffer the poor recognition efficiency, multistep operations and cross-linking reactions. Therefore, novel strategies with efficient phosphate groups recognition and intensified ECL generation are still in high demand.

Bimetallic nanoparticles are critically important in catalysis and electrocatalysis based systems (He et al. 2017; Joseph et al. 2007). They show superior electronic and catalytic properties due to synergistic effects compared to the corresponding homologous monometal nanoparticles (Chen et al. 2012). Amongst various bimetal nanoparticles, Au and Pt bimetallic nanoparticles exhibit outstanding performance in sensing fields, ascribed to their extraordinary catalytic activities, good conductivity and favorable biocompatibility, etc (Qi et al. 2016; Zhang et al. 2017). For instance, bimetallic Au and Pt nanoparticles were investigated in detection of H_2O_2 (Yu et al. 2015), Nitrite (Yang et al. 2016), metal ions (Bu et al. 2015), small organic molecules (Liu et al. 2015b), etc (Wang et al. 2016). Moreover, bimetallic Au and Pt nanoparticles were utilized in an ECL sensor for their ability to enhance the ECL signals of luminol (Shan et al. 2016). However, metal nanoparticles are prone to aggregation during catalytic reactions because of their high surface energy. As a class of crystalline porous materials, metal-organic frameworks (MOFs) featured ordered structures, controllable porosities and large internal surface areas are appropriate candidate to prevent the agglomeration of nanoparticles (Meilikhov et al. 2010). For example, Pd nanoparticles have been loaded into alkyne functionalized MOFs for heterogeneous catalysis (Gole et al. 2016). Pt-Co bimetallic nanoparticles encapsulated within MOFs with controllable size and spatial distribution have been synthesized (Chang and Li 2017). Besides, the pores inside MOFs provide numerous

channels to improve the species diffusion (Yang et al. 2017), affording great potential in sensing applications. Particularly, MOFs hybrids that decorate with metal nanoparticles (NPs@MOFs) can offer great possibilities in designing new signal transductions due to their exceptional tunability (Lei et al. 2014). For instance, AuNPs decorated Ce based MOFs were designed as nanocarriers in an electrochemical strategy, during which AuNPs were utilized to capture SH terminated probes while Ce based MOFs acted as catalysts (Shen et al. 2016b). Besides the ultrahigh porosities and large internal surface areas, NPs@MOFs based sensing systems can benefit from their numerous reactive sites for guest species adsorption or reaction (Wu et al. 2013), thus improve the performances.

In this work, a novel ECL strategy for PKA activity detection and inhibition screening based on Au&Pt@UiO-66 nanocomposites was developed, in which the bimetallic Au and Pt nanoparticles acted as electrocatalysts to improve the ECL signal and the UiO-66 was used as the carriers for bimetallic nanoparticles and the anchorages for phosphate groups. Using PKA as a model, Au&Pt@UiO-66 probes were assembled onto the phosphorylated kemptide modified electrode by forming Zr-O-P bonds between the Zr surface defects on UiO-66 and phosphate groups in phosphorylated kemptide. In addition, the synthesized Au&Pt@UiO-66 nanocomposites not only provided multiple electroactive sites to catalyze the luminol-H_2O_2 ECL reaction, but also afforded numerous Zr defect sites for high efficient phosphate groups recognition. Thus the ECL intensity of the sensing system was significantly improved, affording a sensitive, stable and universal platform for kinase activity analysis and inhibitor screening.

2. Material and methods

2.1. Materials and reagents

Cysteine-terminated kemptide (CLRRASLG) was obtained from GL Biochem (Shanghai, China). PKA (catalytic subunit from bovine heart), ATP and hemoglobin were obtained from Dingguo Biological Products Company (China). Luminol, 4,4′,5,5′,6,6′-hexahydroxydiphenic acid 2,6,2′,6′-dilactone (ellagic acid),

N-(3-chlorophenyl)-6,7-dimethoxy-4-quinazolinamine (Tyrphostin AG1478), anacradic acid, Forskolin and 3-isobutyl-1-methylxantine (IBMX) were purchased from Sigma. Zirconium chloride ($ZrCl_4$), 1,4-benzenedicarboxylic acid (BDC), and N, N-Dimethylformamide (DMF) were purchased from Aladdin Chemistry Co., Ltd (Shanghai, China). $HAuCl_4 \cdot 3H_2O$ (48% w/w) was obtained from Shanghai Reagent (Shanghai, China). Other regents of analytical grade were provided by Beijing Chemical Company (China).

2.2. Apparatus and characterization

The ECL measurements were carried out on a MPI-B multifunctional electrochemical analytical instrument (Xi'an Remex Analytical Instrument Ltd. Co., China) in the electrolyte of 0.1 M PBS containing 0.1 M luminol and 0.1 M H_2O_2. If no special statements, the voltage of photomultiplier tubes (PMT) was maintained at 600 V. The cyclic voltammetry was conducted on a CHI 660b instrument (CH Instrument Co.). The electrochemical cell was in a typical three-electrode configuration using the modified electrode as working electrode, platinum wire as counter electrode and Ag/AgCl, saturated KCl as reference electrode. Electrochemical impedance spectroscopy (EIS) was conducted on SP-150 (Bio-Logic, France) in 0.1 M KCl containing 5 mM of $K_3[Fe(CN)_6]/K_4[Fe(CN)_6]$ with the frequency range from 0.1 Hz to 100 kHz. Scanning electron microscope (SEM) image was obtained with Hitachi SU8000 (Japan). Transmission electron microscope (TEM) and energy-dispersive X-ray (EDX) elemental mapping images were all recorded on Tecnai G2 F30 (FEI, USA).

2.3. Preparation of Au&Pt@UiO-66 nanocomposites

The synthesis process of Au&Pt@UiO-66 nanocomposites was as follows. Firstly, Pt loaded UiO-66 (Pt@UiO-66) was synthesized following a modified protocol reported before (Xu et al. 2015). Briefly, 120 mg of $ZrCl_4$, 96 mg of BDC and 4 mL CH_3COOH were dissolved in 32 mL of DMF with stirring for 10 min. Then 1 mL as-prepared platinum nanoparticles suspension (Fig. S1) was added into the solution, following with ultrasonic treatment. Afterward, the homogeneous mixture was

transferred into a 40 mL Teflon-lined stainless steel autoclave and maintained at 120 °C for 24 h. After cooling down to room temperature, the resultant suspension of Pt@UiO-66 particles was collected by centrifugation. In order to exchange DMF, the ultimately Pt@UiO-66 sample was soaked in alcohol solution for 48 h with stirring. Finally, the product was washed and dried in high dynamical vacuum at 100 °C for hours (Fig. S2).

Au&Pt@UiO-66 nanocomposites were synthesized by chemical reduction of Au^{3+} ions in Pt@UiO-66. Typically, 0.1g Pt@UiO-66 powder was suspended in 100 mL of 0.01% (w/v) $HAuCl_4$ solution with gently stirring for 36 h. And then, the mixture was boiled, followed by addition of 1.5 mL 1% (w/v) trisodium citrate solution. When the solution changed to light purple, indicating the formation of Au&Pt@UiO-66. After the reactor was cooled to room temperature, the synthetic Au&Pt@UiO-66 nanocomposites were collected by centrifugation. After washing with deionized water, the as-synthesized product was dried and characterized by SEM, TEM and EDX elemental mapping.

2.4. Biosensor fabrication

The glassy carbon electrode (GCE) was polished carefully with 0.05 μm Al_2O_3 powder on fine abrasive paper. Then the electrode was washed with distilled water and ethanol, respectively. After drying with N_2, 10 μL graphene oxide (GO) solution was dropped on the GCE surface to provide active sites for anchoring the substrate. Prior to immobilization of kemptide, the GO/GCE electrode was immersed in a freshly prepared solution of 10mM EDC and 10mM NHS for 1h. Afterwards, it was immersed into a PBS (10 mM, pH 7.4) solution containing 500 μM cysteine terminated kemptide in darkness for 12h at room temperature. After washing by PBS solution, the electrode was immersed in 1 mM 6-aminohexanoic acid solution for 30 min to block the electrode. The PKA-catalyzed phosphorylation reaction was performed by incubating the kemptide modified GO/GCE electrode in a PBS solution (50 mM Tris-HCl and 20 mM $MgCl_2$, pH 7.4) containing a desired amount of PKA and ATP for 80 min at 37 °C in an incubator. Finally, the phosphorylated kemptide

modified electrode (phosphorylated kemptide/GO/GCE) was incubated in the solution containing Au&Pt@UiO-66 probes and left standing for 90 min at 37 °C. After finishing the reaction, the resulted electrode (Au&Pt@UiO-66/phosphorylated kemptide/GO/GCE) was thoroughly washed to remove the nonspecific Au&Pt@UiO-66, then the well-assembled biosensor was ready for ECL characterization.

2.5. Preparation of MCF-7 cell lysates

MCF-7 cells (1×10^5) were cultured in DMEM medium supplement at 37 °C under a humidified atmosphere containing 5% CO_2. Before stimulation, serum-free medium was used to replace the previous culture medium. After being starved for 4 h, MCF-7 cells were treated with Forskolin and IBMX solution for activating the intracellular PKA activity. For comparison, ellagic acid solution for inhibiting PKA activity and PBS buffer solution as a control were also added into the medium with final concentration at 25 μM respectively. After stimulation, the cultured MCF-7 cells were treated with lysis buffer for 5 min, then the cell lysates were clarified by centrifugation at 12,000 rpm. Finally, the resulting supernatants were stored at -80 °C and were ready for the subsequent experiments.

3. Results and Discussion.

3.1. Protein kinase activity evaluation

The proposed ECL strategy for PKA activity detection based on bimetallic catalysis signal amplification and recognition of Au&Pt@UiO-66 nanocomposites is demonstrated in Scheme 1. The cysteine-terminated kemptide was firstly assembled on the GO/GCE electrode through the reaction between carboxyl group of the GO and the amino group on the kemptide. Then the kemptide/GO/GCE was treated with 6-aminohexanoic acid for blocking blank binding sites. In the presence of PKA, the hydroxyl group of serine residue in kemptide was replaced by the γ-phosphoryl from ATP. As a result, Au&Pt@UiO-66 probes were modified on the electrode by forming Zr-O-P bonds between Zr-O clusters on UiO-66 and phosphate groups in

phosphorylated kemptide, which were verified by our previous work (Wang et al. 2017). The ECL signal could be improved obviously owing to the excellent catalytic activity of bimetallic Au and Pt nanoparticles. They catalyzed the luminol-H_2O_2 ECL reaction by accelerating the decomposition of H_2O_2 to produce $OH^{\bullet}$ and $O_2^{\bullet -}$, which could activate the oxidation of luminol. Thus light was emitted when the activated luminol ions returned to their ground state (Li et al. 2007; Wei and Wang 2013). Besides, UiO-66 can stabilize the bimetallic nanoparticles during the catalytic reactions and provides more active sites for phosphate group recognition. In addition, the ECL signal was also benefited from the large surface areas and high porosities of Au&Pt@UiO-66 nanocomposites, which not only prompted the electron transfer on the electrode interface but also afforded multiple electroactive centers for reaction. Therefore, the as designed ECL biosensor provides a sensitive tool for kinase activity evaluation.

Scheme 1.

3.2. Characterization of Au&Pt@UiO-66 nanocomposites

Au&Pt@UiO-66 nanocomposites play important roles in enhancing ECL signals and recognizing phosphate groups in the proposed sensing platform. The morphological character of the synthesized Au&Pt@UiO-66 samples was confirmed. Fig.1 and Fig. S3 showed the TEM and SEM images of Au&Pt@UiO-66 nanocomposites, respectively. It could be clearly observed that the well-dispersed Au&Pt@UiO-66 resembled a regular octahedron-like shape with average diameter of 180 nm. It was worth mentioning that encapsulation of bimetallic nanoparticles did not disrupt the crystal structure of UiO-66. Fig.1A depicted that the Au and Pt bimetallic nanoparticles encapsulated in UiO-66 crystal were spherical with an average size of 20 nm. In addition, the corresponding EDX elemental mapping images of Zr, Au and Pt in Au&Pt@UiO-66 (Fig.1B,C and D) and the EDX analysis (Fig. S4) were performed to investigate the elemental compositions of the Au&Pt@UiO-66 probes.

These images pointed to the distribution and dominant peaks of Zr, Au and Pt respectively, further confirmed the successful synthesis of Au&Pt@UiO-66 nanocomposites.

Fig.1.

3.3 Characterization of the biosensors

Fig.2A shows the EIS of bare GCE (curve a), GO/GCE (curve b), kemptide/GO/GCE (curve c), phosphorylated kemptide/GO/GCE (curve d), Au&Pt@UiO-66/phosphorylated kemptide/GO/GCE (curve e) and UiO-66/phosphorylated kemptide/GO/GCE (curve f) in $[Fe(CN)_6]^{4-/3-}$ solution in the frequency range from 0.1 Hz to 100 kHz. EIS is a useful tool that can give information on the impedance changes of the electrode surface during modification. The semicircle diameter of EIS equals the resistance to electron transfer (R_{ct}), reflects the electron transfer kinetics of the redox-probe on the electrode interface. As shown in Fig. 2A, the bare GCE exhibited a small R_{ct}. When the GO was deposited on the electrode, an increase was observed (curve b). After incubating in kemptide solution, the EIS of the resulting assembled layer showed a higher R_{ct} owing to the fact that the kemptide increased the steric hindrance effect, hence obstructed the approach of redox probe to electrode surface (curve c). The diameter of semicircle successively increased after kemptide was phosphorylated by PKA, corresponding to a higher electron-transfer resistance at the electrode interface (curve d). This is because hydroxide group of kemptide was replaced by phosphate group which increased the negative charge density. When treated with Au&Pt@UiO-66 probes, the R_{ct} of the resulted electrode exhibited slight change (curve e), indicating the successful fabrication of the ECL biosensor. Moreover, the R_{ct} of the Au&Pt@UiO-66 treated electrode was lower than that of UiO-66 treated electrode (curve f), owing to the excellent conductivity of Au and Pt bimetallic nanoparticles which promoted the electron transfer of $[Fe(CN)_6]^{4-/3-}$. In addition, the surface coverage (θ_E) of kemptide on the electrode was calculated to be 56% according to the equation below:

$$\theta_{E\ kemptide} = (1 - R_{et} / R_{et}^{kemptide}) \times 100\% \quad (1)$$

where R_{et} is the charge transfer resistance of the GO/GRE surface, and $R_{et}^{kemptide}$ is the corresponding resistance of kemptide immobilized surface.

Fig. 2B presents the ECL emission as a function of potential on the modified electrodes. As it was shown, for the bare GCE (curve a) and kemptide/GO/GCE (curve b), there is a negligible ECL response. After phosphorylated by PKA, similar results were obtained (curve c). For the kemptide/GO/GCE treated with Au&Pt @UiO-66 probes (curve d), it presented a very weak ECL signal since the Au&Pt@UiO-66 couldn't be adsorbed onto the kemptide without phosphorylation. When Au&Pt@UiO-66 was modified on the phosphorylated kemptide modified electrode through the formation of Zr-O-P bonds, a remarkable increase of ECL signal could be observed (curve e), demonstrating the excellent electrocatalytic activity of Au&Pt@UiO-66 toward luminol-H_2O_2 reaction.

To demonstrate the synergistic catalytic effect of the bimetallic Au&Pt@UiO-66 probes for PKA activity analysis and inhibition evaluation, the ECL performances of phosphorylated kemptide modified electrodes treated with UiO-66 (curve a, Fig. 2C), Pt@UiO-66 (curve b, Fig. 2C) and Au&Pt@UiO-66 (curve c, Fig. 2C) were investigated. It was clear that the ECL signal from the Au&Pt@UiO-66 treated electrode was much larger than that of Pt@UiO-66 and UiO-66, indicating the enhanced catalysis ability of Au and Pt bimetallic nanoparticles loaded in UiO-66. Additionally, the stability of the designed biosensor was also evaluated by assaying the PKA activity of 0.15 U mL^{-1}, the ECL signal nearly didn't change after 20 cycles. The relative standard deviation was 5.87%, demonstrating the remarkable stability of the ECL biosensor (Fig. 2D).

Fig.2.

3.4. Optimization of the detection conditions

The concentration of ATP is a crucial parameter for PKA-catalyzed phosphorylation process. As shown in Fig. S5A, the ECL intensity increased with the increasing of ATP concentration and then reached equilibrium at 80 μM. Thus, 80 μM ATP was chosen in the PKA activity study. The phosphorylation time has also been assayed. From Fig. S5B, with the increasing phosphorylation time, the photocurrent signal increased accordingly and reached a maximum level at 80 min, suggesting the complete phosphorylation process. Therefore, 80 min for phosphorylation has been employed in the subsequent experiments. In addition, Au&Pt@UiO-66 were utilized as the ECL signal probe and phosphate groups capture reagent, thus the time for Au&Pt@UiO-66 incubating on modified electrode was critically important. As can be seen from Fig. S5C, the optimal time for Au&Pt@UiO-66 probes incubating on the phosphorylated kemptide was 90 min, thus 90 min was chosen as the appropriate incubation time throughout the study.

3.5. Measurements of PKA activity

To evaluate the activity of PKA, the assessment was carried out under the above-mentioned optimized conditions. Fig. 3A illustrated the ECL signals as a function of times under potential scanning at different concentrations of PKA. The intensity of the ECL peak increased with the increase of PKA concentrations. Fig. 3B and Fig. S6 shows the ECL intensities and the rations of signal/noise at different concentrations of PKA. The ECL signal intensities increased with increasing activity of PKA from 0.015 U mL^{-1} to 60 U mL^{-1}. As shown in the inset of Fig. 3B, the ECL intensity was proportional to the PKA activity in the range from 0.015 U mL^{-1} to 0.25 U mL^{-1} with a correlation equation of I_{ECL} =2516 × C_{PKA}+6.69, where I_{ECL} was the ECL intensity and C_{PKA} was the kinase activity. The corresponding detection limit for PKA was estimated to be 0.009 U mL^{-1} (S/N=3), which showed comparable performance compared with previous reported assays (Table. S1), suggesting that the proposed ECL biosensor based on bimetallic catalysis of Au&Pt@UiO-66 could be applied to sensitive PKA activity analysis.

Fig.3.

The reproducibility of the proposed ECL strategy was evaluated by detecting the same level of PKA activity of 0.15 U mL^{-1} using 6 repeatedly fabricated biosensors. The relative standard deviation was 4.52%, indicating the acceptable reproducibility. To study the selectivity of the ECL biosensor, different enzymes and protein (BSA, glucose oxidase and hemoglobin) on the sensitivity of the biosensor were tested (Fig. S7), and the results showed good selectivity of the proposed platform.

3.6. PKA activity inhibition evaluation and PKA activity detection in cell lysates

The inhibition effects of ellagic acid, a cell-permeable inhibitor of PKA, Tyrphostin AG 1478, a tyrosine kinase inhibitor and anacradic acid, a histone acetyltransferases (HATs) inhibitor have been investigated and compared through the proposed ECL strategy. To evaluate the inhibition effects, the assays were carried out with kinase inhibitors at different concentrations. Curve a in Fig. 4A showed that the ECL intensity decreased with increasing concentrations of ellagic acid and then reached a stable level, indicating the inhibition effect of ellagic acid to the PKA activity. The half-maximal inhibition values (IC50) was calculated to be 3.98 μM, which was consistent with previous results (Yan et al. 2015), indicating the developed ECL biosensor was suitable for inhibitor screening. In addition, the PKA activity analysis was conducted in the presence of Tyrphostin AG 1478 and anacradic acid. As it was shown in curve b and curve c of Fig. 4A, the ECL signal exhibited negligible change with the concentration change of Tyrphostin AG 1478 and anacradic acid. These results clearly demonstrated that the ECL method affords a sensitive, rapid way in quantitative kinase inhibitors screening.

PKA plays crucial regulation roles in protein phosphorylation process, and has a great influence on cell activities. Thus the detection of PKA activity in cells lysates under certain stimulation is necessary. Herein, MCF-7 cells was chosen and stimulated by the Forskolin/ IBMX and ellagic acid, respectively. As shown in Fig. 4B, the ECL response induced by the MCF-7 cell lysate with Forskolin/IBMX stimulation increased, demonstrating the activated PKA activity. On the contrary, the cell lysate stimulated with ellagic acid exhibited the lowest PKA activity. The results were also

comparable with those by ELISA measurements (Fig. S8). These results suggested that the proposed Au&Pt@UiO-66 based ECL biosensor is feasible for kinase analysis in cell samples.

Fig.4.

4. Conclusions

In conclusion, a sensitive ECL biosensor for kinase activity evaluation based on one-step recognition and signal amplification strategy of Au&Pt@UiO-66 nanoprobes has been developed for kinase activity and inhibition assay. The majority of Zr surface defect sites afforded the high efficient recognition toward the phosphorylated kemptide. Moreover, the Au&Pt@UiO-66 not only provided multiple catalytic centers toward the luminol-H_2O_2 reaction but also accelerated the electron transfer rate on the electrode interface. This proposed ECL biosensor showed excellent stability and offered a highly sensitive strategy for PKA activity evaluation with a low detection limit of 0.009 UmL^{-1}. In addition, the proposed ECL biosensor was successfully applied in PKA activity detection and inhibitor screening in cell samples. Therefore, it shows great potential in protein kinase related researches as well as NPs@MOFs related sensing platforms.

Acknowledgments

This work was financially supported by National Natural Science Foundation of China (No. 21622506, 21375073, 21621003, 21235004), National Key Research and Development Program of China (No.2016YFA0203101), Beijing Municipal Science and Technology Commission (Z171100001117135), Tsinghua University Initiative Scientific Research Program (2014z21027), China Postdoctoral Science Foundation (2017M610805) and Beijing Postdoctoral Research Foundation (2017-22-077).

Reference

Bu, L.J., Liu, J., Xie, Q.J., Yao, S.Z., 2015. Electrochem. Commun. 59, 28-31.
Chang, L.N., Li, Y.W., 2017. Mol. Catal. 433, 77-83.
Chen, K.J., Pillai, K.C., Rick, J., Pan, C.J., Wang, S.H., Liu, C.C., Hwang, B.J., 2012. Biosens. Bioelectron. 33, 120-127.
Colombo, S., Broggi, S., Collini, M., D'Alfonso, L., Chirico, G., Martegani, E., 2017. Biochem. Biophys. Res. Commun. 487, 594-599.
Evcimen, N.D., King, G.L., 2007. Pharmacol. Res. 55, 498-510.
Gole, B., Sanyal, U., Banerjee, R., Mukherjee, P.S., 2016. Inorg. Chem. 55, 2345-2354.
Hardie, D.G., 2008. FEBS Lett. 582, 81-89.
He, Q., Shyam, B., Nishijima, M., Yang, X., Koel, B., Ernst, F., Ramaker, D., Mukerjee, S., 2017. J. Phys. Chem. C. 117, 1457-1467.
Hennrich, M.L., Marino, F., Groenewold, V., Kops, G.J., Mohammed, S., Heck, A.J., 2013. J. Proteome Res. 12, 2214-2224.
Hughes, T., Deininger, M., Hochhaus, A., Branford, S., Radich, J., Kaeda, J., Baccarani, M., Cortes, J., Cross, N.C., Druker, B.J., 2006. Blood. 108, 28-37.
Hunter, T., 2000. Cell. 100, 113-127.
Ji, Z.P., Hu, H.G., Yan, B.Y., Zhu, G.X., Xu, Q., Hu, X.Y., 2017. Chin. J. Anal. Chem. 45, 397-402.
Joseph, T., Kumar, K.V., Ramaswamy, A.V., Halligudi, S.B., 2007. Catal. Commun. 8, 629-634.
Lei, J., Qian, R.C., Ling, P.H., Cui, L., Ju, H.X., 2014. TrAC, Trends Anal. Chem. 58, 71-78.
Li, Y.X., Yang, P., Wang, P., Wang, L., 2007. Anal. Bioanal. Chem. 387, 585-592.
Liu, J.Q., He, X.X., Wang, K.M., He, D.G., Wang, Y.H., Mao, Y.F., Shi, H., Wen, L., 2015a. Biosens. Bioelectron. 70, 54-60.
Liu, X., Dong, M.M., Qi, H.L., Gao, Q., Zhang, C.X., 2016. Anal. Chem. 88, 8720-8727.
Liu, X., Li, Y., Xu, X.H., Li, P., Nie, Z., Huang, Y., Yao, S.Z., 2014. TrAC, Trends Anal. Chem. 58, 40-53.
Liu, Y., She, P., Gong, J., Wu, W., Xu, S., Li, J., Zhao, K., Deng, A., 2015b. Sens. Actuators, B. 221, 1542-1553.
Meilikhov, M., Yusenko, K., Esken, D., Turner, S., Van Tendeloo, G., Fischer, R.A., 2010. Eur. J. Inorg. Chem. 2010, 3701-3714.
Meng, L., Wang, Z.Y., Zhang, C.Y., 2016. Chin. J. Anal. Chem. 44, 1934-1941.
Nishizuka, Y., 1986. Nature. 308, 693-698.
Qi, Y.Y., Xiu, F.R., Zheng, M.F., Li, B.X., 2016. Biosens. Bioelectron. 83, 243-249.
Salminen, A., Kaarniranta, K., Haapasalo, A., Soininen, H., Hiltunen, M., 2011. J. Neurochem. 118, 460-474.

Shan, S.M., Mei, S.W., Li, Y.M., Xiao, J.H., Hong, Y., 2016. Talanta. 158, 142-151.

Shen, C.C., Li, X.Z., Rasooly, A., Guo, L.Y., Zhang, K.N., Yang, M.H., 2016a. Biosens. Bioelectron. 85, 220-225.

Shen, C.C., Xia, X.D., Hu, S.Q., Yang, M.H., Wang, J.X., 2015. Anal. Chem. 87, 693-698.

Shen, W.J., Zhuo, Y., Chai, Y.Q., Yuan, R., 2016b. Biosens. Bioelectron. 83, 287-292.

Wang, X.Y., Hu, Y.H., Wei, H., 2016. Inorg. Chem. Front. 3, 41-60.

Wang, Z.H., Yan, Z.Y., Wang, F., Cai, J.B., Guo, L., Su, J.K., Liu, Y., 2017. Biosens. Bioelectron. 97, 107-114.

Wei, H., Wang, E.K., 2013. Chem. Soc. Rev. 44, 6060-6093.

Whiteman, E.L., Han, C., Birnbaum, M.J., 2002. Trends Endocrinol. Metab. 13, 444-451.

Whitmarsh, A.J., 2007. Biochim. Biophys. Acta, Mol. Cell Res. 1773, 1285-1298.

Xu, Z.D., Yang, L.Z., Xu, C.L., 2015. Anal. Chem. 87, 3438-3444.

Yan, Z.Y., Wang, Z.H., Miao, Z., Liu, Y., 2015. Anal. Chem. 88, 922-929.

Yang, C.Y., Chen, S.M., Palanisamy, S., Thirumalraj, B., Liu, X., 2016. Int. J. Electrochem. Sci. 11, 4027-4036.

Yang, Q.H., Xu, Q., Jiang, H.L., 2017. Chem. Soc. Rev. 46, 4774-4808.

Yu, G., Wu, W., Pan, X., Zhao, Q., Wei, X., Lu, Q., 2015. Sensors. 15, 2709-2722.

Zhang, H., Buckley, N.E., Gibson, K., Spiegel, S., 1990. J. Biol. Chem. 265, 76-81.

Zhang, X., Ke, H., Wang, Z.M., Guo, W.W., Zhang, A.M., Huang, C.S., Jia, N.Q., 2017. Analyst. 142, 2253-2260.

Zhao, H.F., Liang, R.P., Wang, J.W., Qiu, J.D., 2015. Chem. Commun. 51, 12669-12672.

Zhou, J., Xu, X.H., Liu, X., Li, H., Nie, Z., Qing, M., Huang, Y., Yao, S.Z., 2014. Biosens. Bioelectron. 53, 295-300.

Zhu, X.Q., Zhai, Q.F., Gu, W.L., Li, J., Wang, E.K., 2017. Anal. Chem. 89, 12108-12114.

Legends

Scheme 1. The configuration of ECL biosensor for kinase activity detection and the mechanism of enhanced luminol ECL catalyzed by Au&Pt@UiO-66.

Figure 1. TEM image (A), The EDX elemental mapping of Zr (B), Au (C), Pt (D) of Au&Pt@UiO-66.

Figure 2. (A) EIS of (a) the bare GCE electrode, (b) GO/GCE, (c) kemptide/GO/GCE, (d) phosphorylated kemptide/GO/GCE, (e) Au&Pt@UiO-66/phosphorylated kemptide/GO/GCE, (f) UiO-66/phosphorylated kemptide/GO/GCE. The spectra were recorded in $[Fe(CN)_6]^{4-/3-}$ solution in the frequency range from 0.1 Hz to 100 KHz. (B) The ECL intensity-potential curves of (a) GCE, (b) kemptide/GO/GCE, (c) phosphorylated kemptide/GO/GCE, (d) kemptide/GO/GCE with the treatment of Au&Pt @UiO-66 probes, (e) the phosphorylated kemptide GO/ GCE with the treatment of Au&Pt @UiO-66 probes. The curves were recorded at scan rate of 100mVS^{-1} in a 0.1M PBS solution containing 100 μM luminol and 0.1 M H_2O_2, the voltage is maintained at 600 V. (C) The ECL intensity response of the phosphorylated kemptide GO/ GCE with the treatment of (a) UiO-66 probes, (b) Pt @UiO-66 probes, (c) the phosphorylated kemptide GO/ GCE with the treatment of Au&Pt @UiO-66 probes. (D) The ECL intensity-time curve of 0.15 U mL^{-1} PKA in the 0.1 M PBS solution containing 100 μM luminol and 0.1 M H_2O_2 for 20 cycles at a scan rate of 100 mV s^{-1}, the voltage is maintained at 600 V.

Figure 3. (A) The ECL intensity-time curves in the 0.1 M PBS solution containing 100 μM luminol, 0.1 M H_2O_2 and PKA with different concentrations. (B) The ECL intensity at different PKA concentrations from 0.015 to 80 U mL^{-1}. The inset is the linear relationship between ECL intensity and PKA concentrations. The scan rate is 100 mV s^{-1}, the voltage is maintained at 600 V.

Figure 4. (A) The ECL intensity of different concentrations of ellagic acid (a) and Tyrphostin AG 1478 (b) and anacradic acid (c). The concentrations of PKA and ATP are 0.25 U mL^{-1} and 100 μM, respectively. (B) The ECL intensity of the PKA

expression in MCF-7 cells lysates stimulated by Forskolin, ellagic acid and PBS buffer, respectively. The error bars represent the standard deviation of three measurements.

Scheme 1

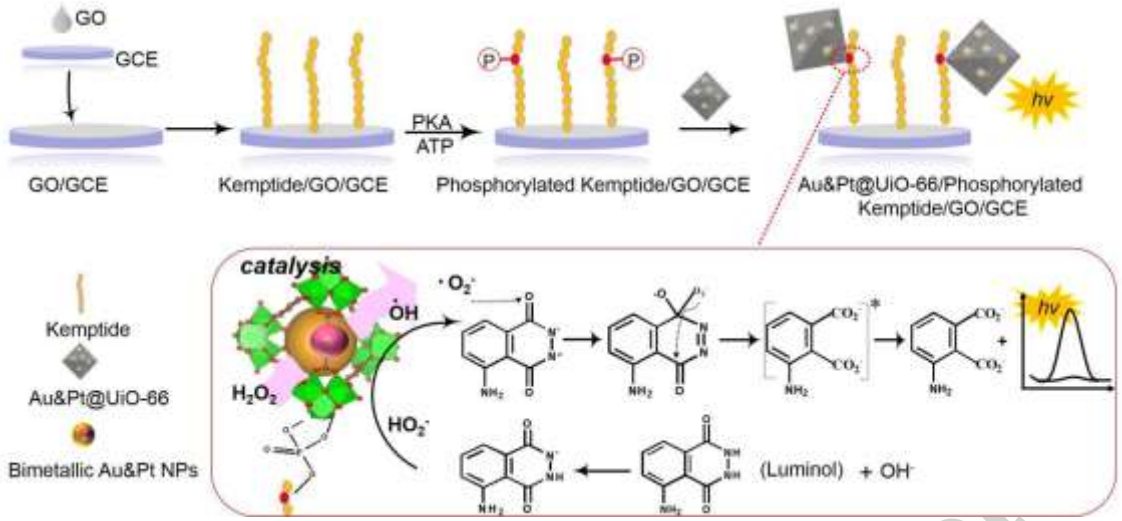

Fig. 1

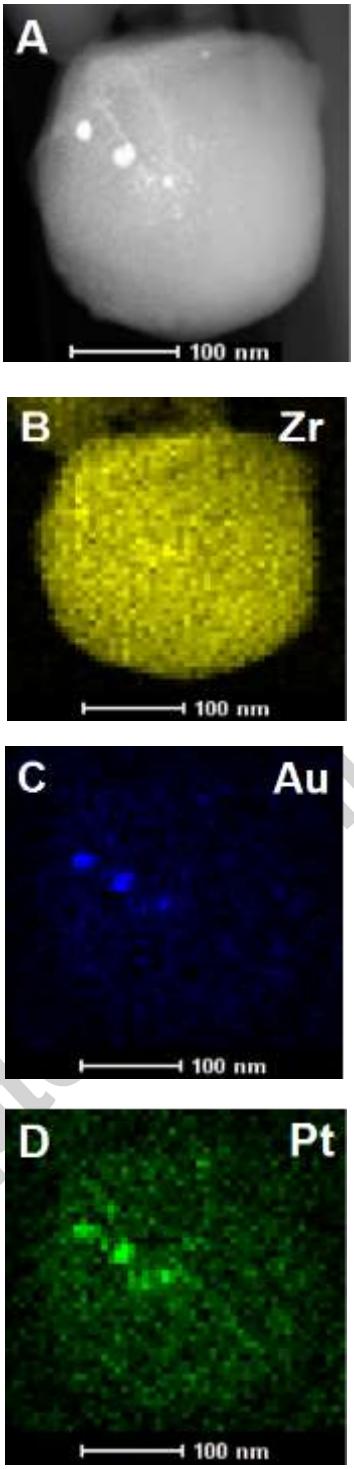

Fig. 2

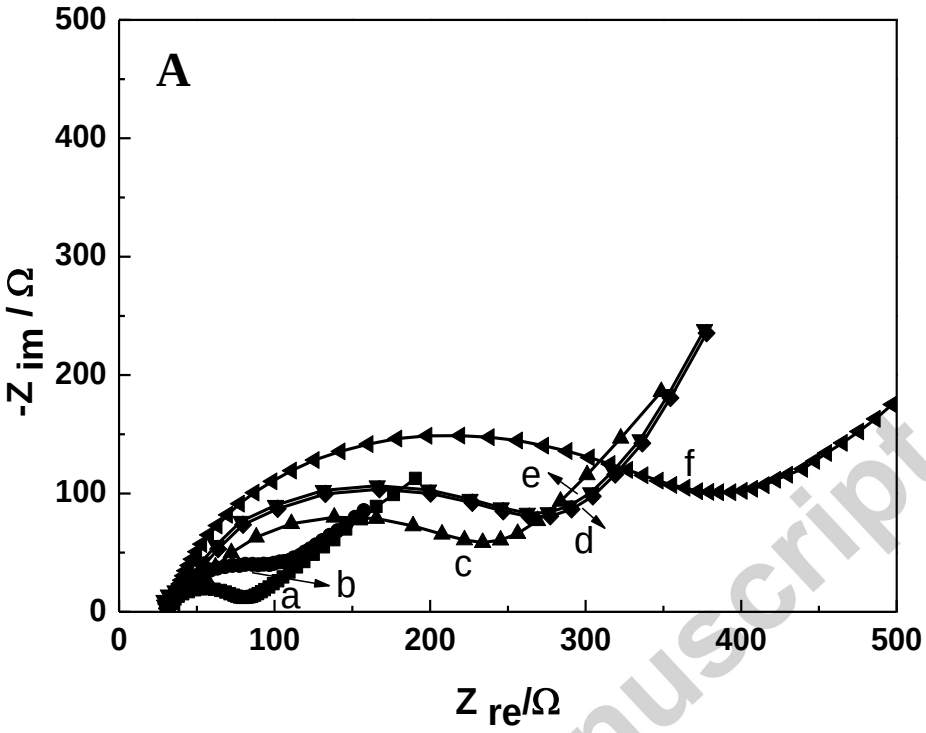

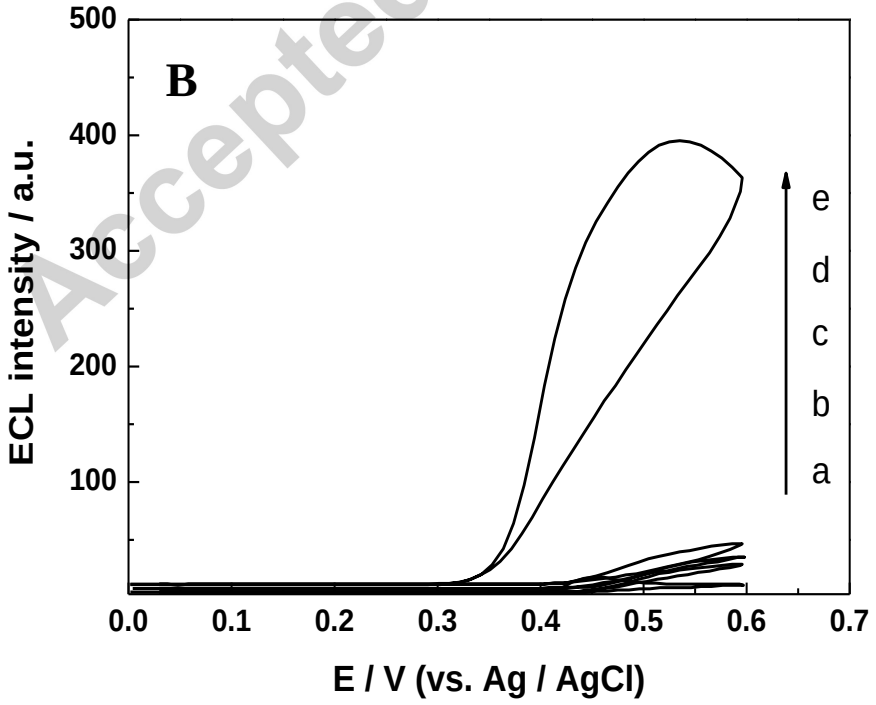

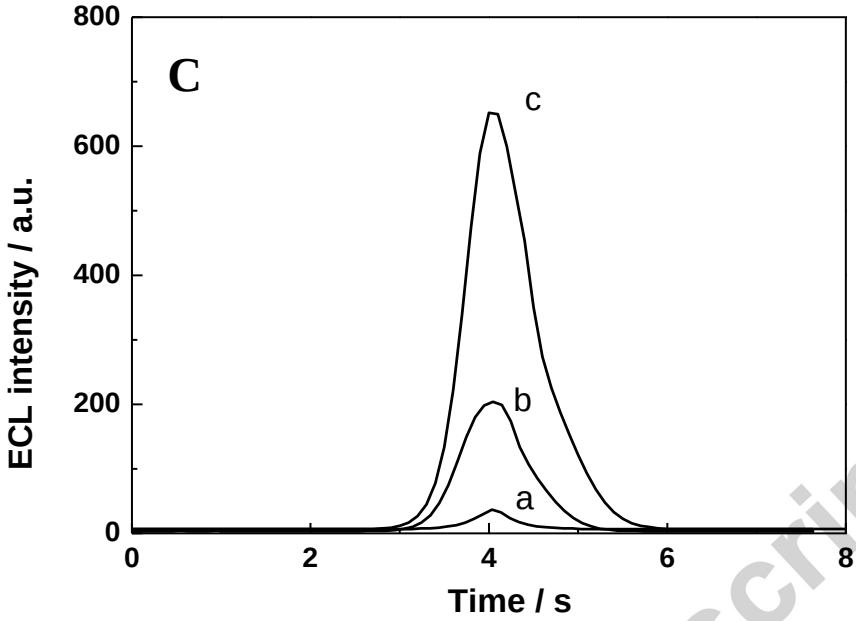

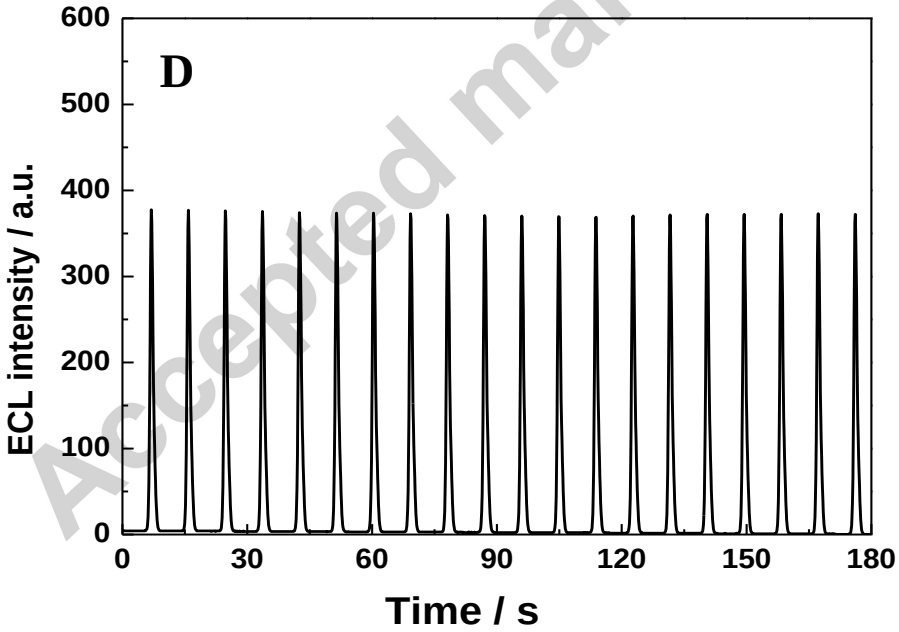

Fig. 3

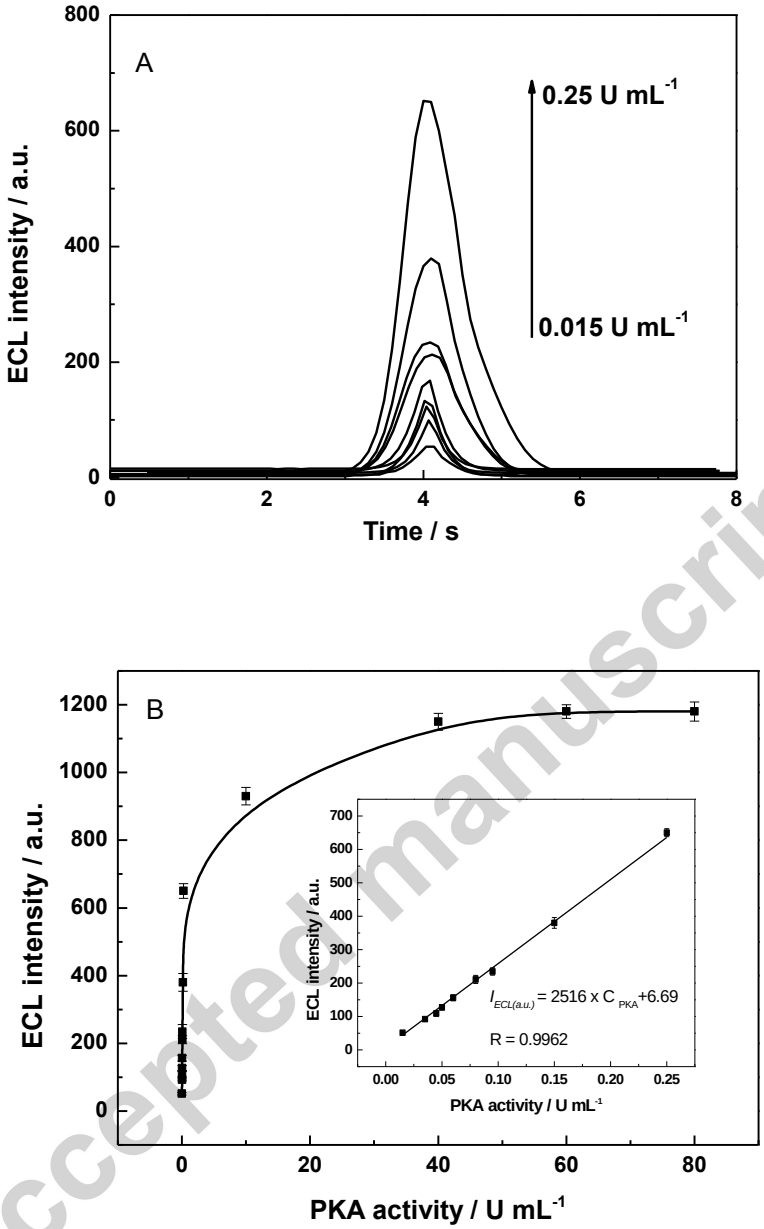

Fig. 4

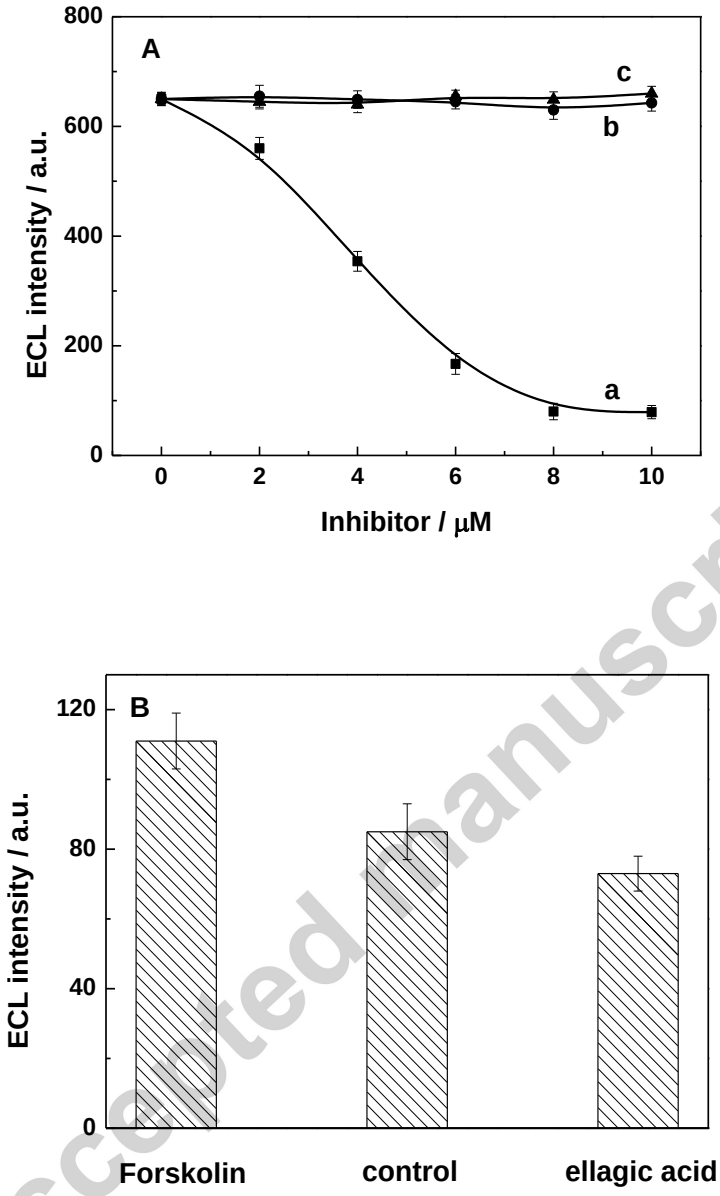

Highlights

1, A novel ECL strategy for PKA activity detection and inhibition screening based on Au&Pt@UiO-66 nanocomposites was developed.

2, The high synergistic catalysis activities of Au&Pt@UiO-66 nanocomposites to the luminol-H_2O_2 reaction and the numerous Zr defect sites UiO-66 for high efficient phosphate group recognition afforded the excellent performances of the ECL biosensor.

3, The uniform porous structure of UiO-66 can prevent the nanoparticles from aggregating and thus superior stability of the biosensor was obtained.

4, The biosensor was applied for quantitative kinase inhibitor evaluation and PKA activities detection in cell lysis samples.